PERSIANN-CNN: Precipitation Estimation from Remotely Sensed Information Using Artificial Neural Networks–Convolutional Neural Networks

MOJTABA SADEGHI

Center for Hydrometeorology and Remote Sensing, Department of Civil and Environmental Engineering, University of California, Irvine, Irvine, California

ATA AKBARI ASANJAN

Center for Hydrometeorology and Remote Sensing, Department of Civil and Environmental Engineering, University of California, Irvine, Irvine, and Universities Space Research Association, Mountain View, California

MOHAMMAD FARIDZAD, PHU NGUYEN, KUOLIN HSU, SOROOSH SOROOSHIAN, AND DAN BRAITHWAITE

Center for Hydrometeorology and Remote Sensing, Department of Civil and Environmental Engineering, University of California, Irvine, Irvine, California

(Manuscript received 20 May 2019, in final form 24 September 2019)

ABSTRACT

Accurate and timely precipitation estimates are critical for monitoring and forecasting natural disasters such as floods. Despite having high-resolution satellite information, precipitation estimation from remotely sensed data still suffers from methodological limitations. State-of-the-art deep learning algorithms, renowned for their skill in learning accurate patterns within large and complex datasets, appear well suited to the task of precipitation estimation, given the ample amount of high-resolution satellite data. In this study, the effectiveness of applying convolutional neural networks (CNNs) together with the infrared (IR) and water vapor (WV) channels from geostationary satellites for estimating precipitation rate is explored. The proposed model performances are evaluated during summer 2012 and 2013 over central CONUS at the spatial resolution of 0.08° and at an hourly time scale. Precipitation Estimation from Remotely Sensed Information Using Artificial Neural Networks (PERSIANN)–Cloud Classification System (CCS), which is an operational satellite-based product, and PERSIANN–Stacked Denoising Autoencoder (PERSIANN-SDAE) are employed as baseline models. Results demonstrate that the proposed model (PERSIANN-CNN) provides more accurate rainfall estimates compared to the baseline models at various temporal and spatial scales. Specifically, PERSIANN-CNN outperforms PERSIANN-CCS (and PERSIANN-SDAE) by 54% (and 23%) in the critical success index (CSI), demonstrating the detection skills of the model. Furthermore, the root-mean-square error (RMSE) of the rainfall estimates with respect to the National Centers for Environmental Prediction (NCEP) Stage IV gauge–radar data, for PERSIANN-CNN was lower than that of PERSIANN-CCS (PERSIANN-SDAE) by 37% (14%), showing the estimation accuracy of the proposed model.

1. Introduction

Precipitation is the main driver of the hydrological cycle, and it plays a key role in hydrometeorological and climate studies (Trenberth et al. 2003). Accurate and timely precipitation estimates are of paramount importance for water resources management, as well as many hydrological applications such as flood forecasting, drought modeling, and soil moisture monitoring (Beck et al. 2017; Miao et al. 2015). Rain gauges, weather radars, and Earth-observing satellites are the most common instruments for estimating precipitation. Ground-based rain gauges provide direct rainfall measurement and are considered the most reliable method for rainfall estimation (Huffman et al. 1997). Yet, the inadequacy and the sparsity of gauge networks over remote and high elevation areas that receive large amounts of precipitation tend to undermine the applicability of gauge-based estimates (Gehne et al. 2016; Huffman et al. 2001). Additionally, there are no gauge data over water bodies and

Corresponding author: Mojtaba Sadeghi, mojtabas@uci.edu

DOI: 10.1175/JHM-D-19-0110.1

oceans (Maggioni et al. 2016). Radar networks provide a continuous precipitation measurement with high temporal and spatial resolutions (Habib et al. 2012). However, radar networks do not cover many countries and remote regions around the world (Guo et al. 2015; Yilmaz et al. 2005). Additionally, they suffer from beam overshooting and beam blockage by mountains, which makes them suitable mostly for flat regions (Germann et al. 2006).

Satellite-based quantitative precipitation estimation (QPE) is a promising alternative to ground-based rain gauge and radar measurements, offering global precipitation estimates with high spatial and temporal resolutions over land surfaces and oceans (Sun et al. 2018). Satellite-based QPEs can be derived from a range of observations with different types of sensors. The most commonly used satellite sensors are infrared (IR) from geosynchronous Earth-orbiting (GEO) satellites and passive microwave (PMW) data from low-Earth-orbiting (LEO) satellites (Michaelides et al. 2009; Sorooshian et al. 2002; Weng et al. 2003). PMW observations have the advantage of being directly retrieved by measuring microphysical information including both liquid and frozen hydrometeors within the clouds, while IR information is limited to cloud-top information (Joyce et al. 2004). PMW sensors are only onboard LEO satellites, which provide a relatively poor temporal and spatial sampling (Behrangi et al. 2009; Marzano et al. 2004). IR images are produced at least once per hour and provide useful information regarding cloud-top texture (e.g., size and phase of cloud particles) (Grecu et al. 2004). In addition, the resolution of IR sensors is around 4 km, while the resolutions of LEO sensors are typically not better than 50 km over the oceans and 10 km over land (Kidd and Levizzani 2011). Thus, the IR-based products have the advantage in terms of temporal and spatial resolutions among other satellite-based QPEs and better meet the requirements many near-real-time applications. Such applications include monitoring the complete evolution of local precipitation events and flash floods, where the life cycle of most storms occurs within a short period of time and is confined to a small area (Arkin and Meisner 1987; Behrangi et al. 2009).

Different methodologies have been proposed in order to establish the relationships between IR observations and precipitation rate (Ba and Gruber 2001; Behrangi et al. 2009; Bellerby et al. 2000; Hsu et al. 1997; Roebeling and Holleman 2009). One well-known algorithm and product is Precipitation Estimation from Remotely Sensed Information Using Artificial Neural Networks (PERSIANN) which relates cloud-top temperature data obtained from IR imagery to the precipitation rate (Hsu et al. 1997). PERSIANN is a near-real-time dataset with 0.25° (i.e., 25 km) spatial and hourly temporal resolutions (Sorooshian et al. 2000). PERSIANN–Cloud Classification System (PERSIANN-CCS; Hong et al. 2004) is the next generation of PERSIANN, which improves the estimation algorithm by employing techniques to identify the cloud patch features. PERSIANN-CCS data are a product at 0.04° (i.e., 4 km) spatial and half-hourly temporal resolutions. Both PERSIANN and PERSIANN-CCS extract information based on manually defined features including coldness, texture, and geometry, which limits the capability of these products for precipitation estimation (Hong et al. 2004; Shen 2018). Manual feature extraction is always limited due to the tendency of humans to select the most relevant and physically obvious features that have a direct impact on a phenomenon. However, due to the complexity and nonlinear behavior of the precipitation phenomena, there may be some factors hidden to humans that play significant roles in increasing the accuracy of simulations. Additionally, in practice, human-based feature selection is biased toward the most obvious factors due to insufficient time to explore and test all related and co-related factors. Therefore, applying more advanced data-driven methodologies for automatically extracting features from the input data will enhance precipitation estimation accuracy.

Recent advances in the field of machine learning (ML) offer exciting opportunities to expand our knowledge about the Earth system (Lary et al. 2016). Among the different machine learning methods, the deep neural network (DNN) method is a fast-growing branch characterized by its flexibility and capacity to deal with huge and complex datasets, especially extracting features from a large amount of image data (Bengio et al. 2007; Hinton et al. 2006). DNN's ability to deal with huge amounts of data allows us to better exploit spatial and temporal structures in the data from multisatellite imageries for precipitation estimation. Akbari Asanjan et al. (2018) employed a deep neural network framework and proposed a short-term quantitative precipitation forecasting model. A more closely related work for applying DNNs for precipitation estimation is the research conducted by Tao et al. (2018), who employed the stacked denoising autoencoders technique. The proposed model, referred to as PERSIANN stacked denoising autoencoders (PERSIANN-SDAE), utilizes IR and water vapor (WV) channels to detect rain/no-rain and then estimate the precipitation. The results suggest that PERSIANN-SDAE can better capture both the spatial pattern and the peak precipitation compared to PERSIANN-CCS. Although PERSIANN-SDAE has the advantage of automatic feature extraction from the IR data, it cannot efficiently use the neighborhood information in retrieving the rain rate at each pixel due to an inefficient structure for learning from image datasets.

In other words, for each output pixel estimated by SDAE and in general Fully connected (FC) neural networks, information from the corresponding pixel of the input datasets is utilized instead of using information from neighboring pixels in the same image. The inefficient structure of SDAE and FC networks leads to results focusing on the pixel-to-pixel relationship between cloud-top temperature and rainfall rate. However, in addition to the one-to-one relation of IR temperature and rain rate, local spatial variations in IR provide useful factors for accurate rainfall estimation. For example, frontal rainfalls can be well described by spatial variations in IR. Frontal rainfalls happen when cold and warm regimes collide, and this is only captured by leveraging spatial patterns.

Convolution neural networks (CNNs) are one of the most popular and efficient types of DNN frameworks (Rezaee et al. 2018). CNNs rely on efficient structures for learning the essential features without requiring prior feature extraction and thereby offer a greater generalization capability (Long et al. 2017). One of the main advantages of CNNs for image processing is that they can more efficiently use local neighborhood features via convolution transformation (Miao et al. 2015). In other words, CNNs use the $n \times n$ neighborhood pixels centered by the targeted pixel to estimate the rain rate at that pixel. This feature is due to the CNN structure, which allows sharing the same filter in a single layer. By offering this unique feature, the CNN can extract valuable features from the hidden layer without requiring large amounts of data. This greatly reduces the number of parameters in the network and allows the model to have more layers (deeper structure), which are good for capturing more complex patterns, and to be more efficient by reducing the number of parameters compared to FC models (Chen et al. 2016).

Due to the rapid growth in the amount of annotated data and the uniqueness of CNN structures, remote sensing and hydrology communities have exploited CNN techniques for many applications. These include land cover and land use classification (Castelluccio et al. 2015; Chen et al. 2014; Luus et al. 2015; Makantasis et al. 2015; Rezaee et al. 2018; Ševo and Avramović 2016), image segmentation (Basaeed et al. 2016; Längkvist et al. 2016), object localization (Long et al. 2017; Salberg 2015), extreme event detection (Liu et al. 2016), urban water flow and water level prediction (Assem et al. 2017), tropical cyclone intensity estimation (Pradhan et al. 2018), and extreme precipitation prediction (Zhuang and Ding 2016). The CNN structure can also be utilized to address the drawback of PERSIANN-SDAE to efficiently utilize neighborhood pixel information for rain-rate estimation (Shen 2018). The CNN offers a viable tool for precipitation estimation problems since it can gain more abstract and more expressive information from multispectral channels. Recently, a CNN was implemented to estimate precipitation based on the dynamic and moisture fields from numerical weather model analysis (Pan et al. 2018). Pan et al. (2018) showed that the CNN technique can improve numerical precipitation estimation on the west and east coasts of United States. Miao et al. (2019) applied a combination of CNN and long short-term memory (LSTM) to improve the resolution and accuracy of precipitation estimates based on dynamical simulations. Both of these studies employ predictions from the numerical model's resolved dynamic and moisture fields. However, there is no remote sensing information being explicitly utilized in their models.

In this study, we propose a framework for real-time precipitation estimation using the IR and WV information and applying a CNN model. The National Centers for Environmental Prediction (NCEP) Stage IV QPE has been utilized as the ground-truth observation for training the model. The proposed model will be called PERSIANN–Convolutional Neural Network (PERSIANN-CNN) hereafter. Then, the effectiveness of this model has been evaluated, and its performance is compared with two baseline models. The detailed objectives of this study are

1) to introduce a rainfall estimation model based on the bispectral satellite information (IR and WV channels) using convolutional neural networks;
2) to evaluate the performance of the proposed model (PERSIANN-CNN) through various categorical and continuous verification indices and contrast the proposed model with PERSIANN-CCS and PERSIANN-SDAE at hourly and daily time scales; and
3) to verify the performance of PERSIANN-CNN in capturing the characteristics of an extreme rainfall event throughout its evolution stages.

The remainder of this paper is organized as follows. Section 2 covers information regarding the utilized data and the study area. Section 3 describes the details of the applied model and evaluation metrics. Section 4 covers the evaluation of the PERSIANN-CNN model and comparison with the baseline models at hourly and daily scales. The main conclusions of this study are summarized in section 5.

2. Data and study area

a. Model inputs and the observational dataset

1) NOAA GOES IMAGERY (IR AND WV)

The input data used in this study are IR and WV channels from Geostationary Operational Environmental

Satellite (GOES) satellites with wavelengths of 10.7 and 6.7 μm, respectively. The WV channel is utilized as a supplementary input to the IR data since previous studies by Ba and Gruber (2001) and Behrangi et al. (2009) have shown the contribution the WV channel can add for rainfall estimation. Physically, the conversion of water vapor is necessary for precipitation formation (Stohl and James 2004). Previous studies have shown that the WV channel in conjunction with IR can recover a great amount of missing precipitation under warm clouds (Kurino 1997; Tao et al. 2017). In this study, both IR and WV channel data from GOES are processed to an hourly scale with a 0.08° (8 km) spatial resolution.

2) NCEP STAGE IV QPE PRODUCT

The NCEP Stage IV QPE is often assumed to be the best long-term precipitation observation over the CONUS due to its extensive quality control procedures and uniform space–time grid (Smalley et al. 2014). This product, hereafter referred to Stage IV, combines the national Weather Surveillance Radar-1988 Doppler (WSR-88D) network of ground radars and surface gauges for precipitation estimation (Lin and Mitchell 2005). For this study, hourly NCEP Stage IV QPE precipitation accumulations at 0.04° (4 km) spatial resolution were obtained from the Stage IV QPE distribution website to serve as the ground-truth observations (http://www.emc.ncep.noaa.gov/mmb/ylin/pcpanl/stage4/). The original 0.04° dataset was resampled to 0.08° (8 km) spatial resolution to match the resolution of the IR and WV data.

b. Baseline models

1) PERSIANN-CCS

PERSIANN-CCS is a near-real-time precipitation estimation at 0.04° spatial resolution and half-hourly temporal resolution and has become popular as an operational product. The PERSIANN-CCS algorithm employs IR satellite imagery to extract local and regional cloud features to estimate rainfall (Hong et al. 2004) in four steps:

1) Cloud segmentation separates IR imagery into distinctive cloud patches using an incremental temperature threshold algorithm.
2) Feature extraction extracts local and regional cloud patch features, including coldness, texture, and geometry.
3) Cloud classification clusters cloud patches into well-organized subgroups using self-organizing feature maps (SOFMS) based on cloud patch features.
4) Rainfall mapping uses cloud-top temperature and rainfall relationships for each classified cloud cluster.

In step 4, the relationship between the cloud-top temperature and the rain rate is obtained for every cluster by applying probability matching method (PMM) and an exponential curve fitting. One of the main advantages of this algorithm is its simplicity and its ability to capture extreme precipitation events (Hong et al. 2004). For this study, PERSIANN-CCS (downloaded from https://chrsdata.eng.uci.edu/) was resampled to a 0.08° spatial resolution and an hourly temporal resolution for the purpose of comparison.

2) PERSIANN-SDAE

Developed by Tao et al. (2018), the PERSIANN-SDAE algorithm uses IR and WV data in a fully connected deep neural network model to detect and estimate the rainfall rate. The SDAE technique, introduced by Vincent et al. (2008), is an unsupervised pretraining method to extract useful information from the input data and is particularly useful for image recognition tasks. The PERSIANN-SDAE algorithm applies a three layer fully connected neural network employing a greedy layer-wise pretraining based on stacked denoising autoencoders utilizing IR and WV channels (Tao et al. 2016, 2017). Kullback–Leibler (KL) divergence and mean square error (MSE) were used as the loss functions in the PERSIANN-SDAE algorithm. These objective functions help decrease estimation error while preserving the distribution of the rainfall. Another advantage of the SDAE algorithm is that it can automatically extract useful features from the input data. This results in a complicated functional mapping between the raw input data and the observational data. On the other hand, traditional neural networks like PERSIANN-CCS use manually designed features for data extraction (Tao et al. 2016), which does not efficiently utilize the neighborhood pixels' information for precipitation estimation of each pixel (Aoki 2017). In this study, we utilize the same dataset for PERSIANN-SDAE that Tao et al. (2016) presented.

c. Study area

The study area of this research is the central United States within the latitudes 30°–45°N and longitudes 90°–105°W (Fig. 1). This region has been chosen primarily because of its predominant convective precipitation mechanism that leads to intense storms during summertime. As a result, many satellite-based precipitation retrieval algorithms experience challenges in detection and estimation of rainfall in the region (Houze 2012). Another reason for choosing

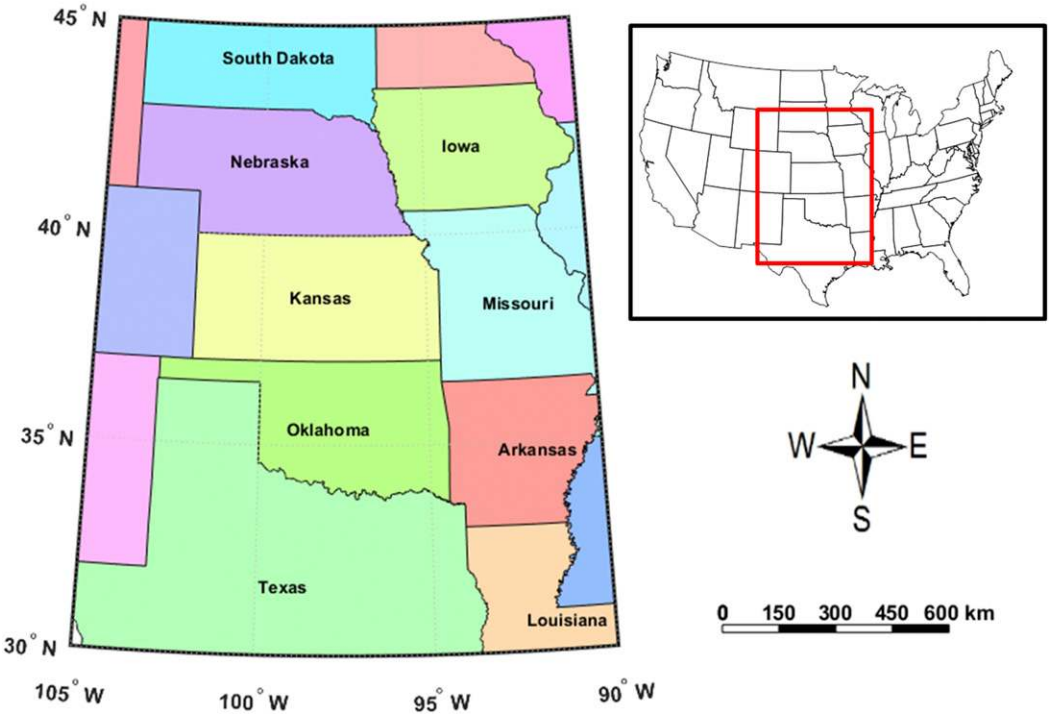

FIG. 1. Map of the study region in the central United States.

this study area is the availability of high quality radar data, which allows for better training and more accurate verification of the models.

3. Methodology

a. CNN architecture

The CNN is one of the most widely used deep learning algorithms, having recently gained much interest in the field of image processing (Zhu et al. 2017). The CNN is superior to other DNN algorithms due to its ability to preserve the spatial information by maintaining the interconnection between pixels (Rezaee et al. 2018). The CNN is one type of feed-forward neural network in which an input passes through one or multiple layers of "neurons." Each neuron represents a linear combination of inputs that passes through a typically nonlinear function, called the activation layer, and then passes to the next layer. The model can then be trained with a backpropagation algorithm (Walker et al. 2015). The goal of training is to update sets of weight matrices and bias vectors to minimize the loss function, that is, the distance between the estimation and observation. A CNN network is typically constructed with one or more convolution layers and pooling layers (Krizhevsky et al. 2012; Shen 2018). In convolution layers, outputs (feature maps) of the previous layer are convolved by sliding convolution filters, which have learnable weights, to

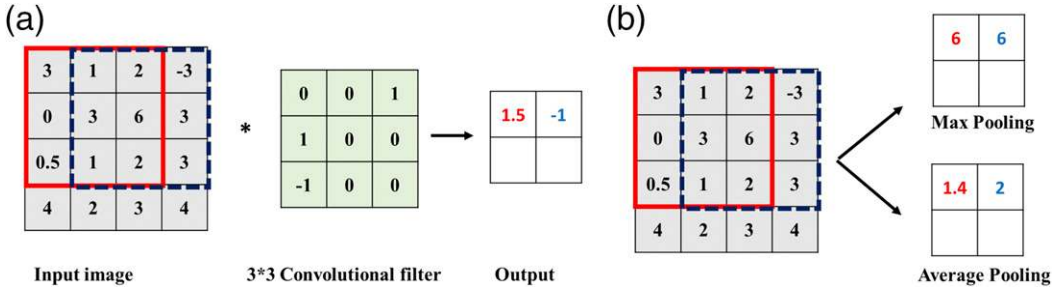

FIG. 2. (a) An example of a 3 × 3 convolutional filter applied to a 4 × 4 matrix; (b) an example of 3 × 3 max-pooling/average-pooling filter applied to a 4 × 4 matrix.

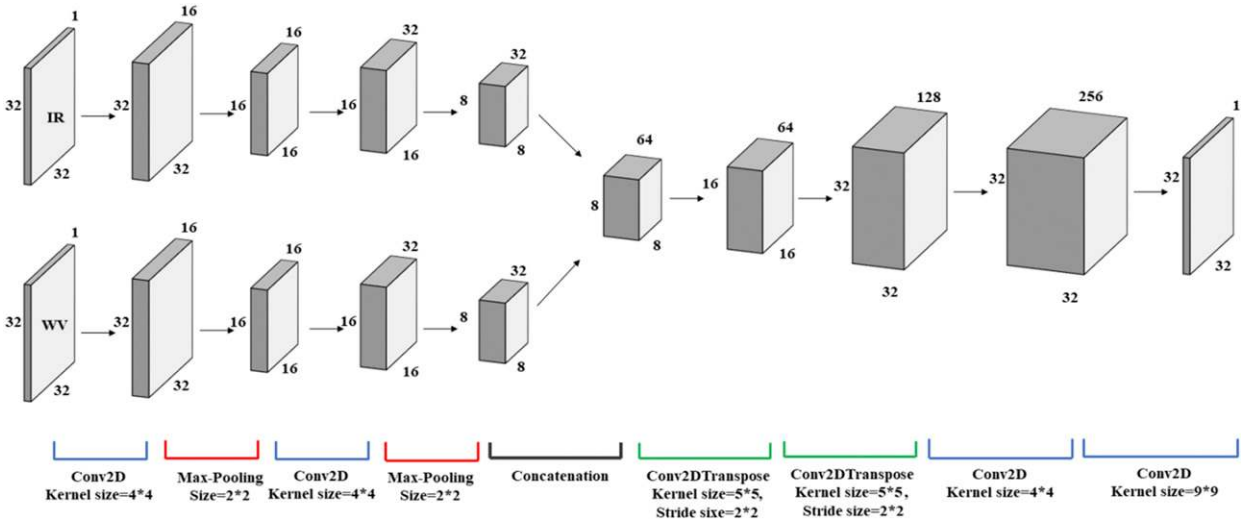

FIG. 3. Schematic of the proposed CNN model.

extract hidden features from the input. Figure 2a represents an example of applying a two-dimensional convolutional filter (Conv 2D) to an input matrix. Each element of the output is obtained from summing the element-wise product of the input matrix and the convolutional filter. The output of the convolution operator is added by a separately trained bias vector. The result is plugged into an activation function to construct the feature map of the next layer (Yang et al. 2015). A convolution layer is often paired with a pooling layer (also called subsampling layer). In the pooling layer, the spatial resolution of feature maps is reduced to decrease the number of parameters; thus decreasing the computation cost and avoiding overfitting. There are many methods for subsampling, such as average pooling and max pooling (Van Doorn 2014). In an average-pooling layer, elements of the input are averaged within a window to form the output, while the maximum element of that window is obtained as the output in a max-pooling layer (Fig. 2b). For this study we utilized max-pooling layers since they can further reduce the scale of the input and greatly decrease the model's dimensionality to avoid overfitting (Walker et al. 2015).

b. Model setup

1) OVERVIEW OF THE LAYERS

The architecture of the proposed CNN model with details of input shape, filter size, stride size and output is shown in Fig. 3. The inputs are two 32×32 matrices containing the IR and WV channels of GOES-West satellite. The inputs are separately convolved in order to learn information from each channel individually. Then, we utilize a concatenation function to merge the two map features. The output can be upsampled from low resolution to high resolution in two steps using a two-dimensional convolutional transpose function (2D ConvTranspose). Then the final feature maps were derived after convolving the output of the previous layers for two times. The output of the model is the rain rate with the same spatial and temporal resolutions as the input data. Furthermore, in all steps we utilize a rectified linear unit (ReLU) activation function for nonlinearity. The ReLU function is $f(x) = \max(0, x)$, (Walker et al. 2015).This function can be quickly computed since it does not have any exponential or multiplication function and assigned zero for negative elements. Furthermore, computing the gradient of the ReLU function is simple and can be either 0 or 1 based on the sign of the element.

2) PARAMETER TUNING

The inputs (IR and WV) and target (Stage IV) datasets are divided into the training, validation, and test periods. Summer 2012 (June–August) and the first month of summer 2013 (June) were used for training and July 2013 was used for validation. The training and validation dataset are utilized to optimize the model parameters and also prevent overfitting. August 2013 was kept unused during the training phase and was used for testing the developed model. Various combinations of the hyperparameters were tested during the training phase of the CNN model to optimize the 869 665 learnable parameters of the proposed model. Hyperparameters are the variables which determine the structure of a DNN (i.e., layer type, neuron size) and the variables that determine how the CNN network should be trained (i.e.,

learning rate) (Erhan et al. 2010). MSE was defined as the loss function to minimize during the training and validation phases. The initial values of the parameters are randomly selected from a standard normal distribution. Then, the parameters are trained using the gradient descent method in order to minimize the errors at each epoch. Also, an early stopping criterion was introduced that halted the training if the objective function value did not improve after 10 epochs. The lowest MSE in both training and validation periods are achieved by defining the model specific hyperparameters leading to the configuration shown in Fig. 3. Furthermore, a learning rate of 0.01, a minibatch size of 32, and an epoch size of 100 were determined through the minimizing processes.

c. *Performance measurements*

1) CATEGORICAL EVALUATION STATISTICS

Categorical evaluation statistics are used to evaluate the abilities of the models in detecting rain/no-rain pixels. These statistical indices include the probability of detection (POD), false alarm ratio (FAR), and the critical success index (CSI). The mathematical formulations for each of these indices are given below:

$$\mathrm{POD} = \frac{\mathrm{TP}}{\mathrm{TP}+\mathrm{MS}} \text{(range: from 0 to 1; desirable value: 1)},$$

$$\mathrm{FAR} = \frac{\mathrm{FP}}{\mathrm{TP}+\mathrm{MS}} \text{(range: from 0 to 1; desirable value: 0)},$$

$$\mathrm{CSI} = \frac{\mathrm{TP}}{\mathrm{TP}+\mathrm{FP}+\mathrm{MS}} \text{(range: from 0 to 1; desirable value: 1)},$$

where TP is the number of pixels correctly classified as rain (true positive events), FP is the number of pixels incorrectly classified as rain (false positive events), and MS is the number of pixels incorrectly classified as no rain (missing events).

2) CONTINUOUS EVALUATION STATISTICS

Continuous indices are employed to evaluate the skill of each algorithm in estimating rainfall intensity. Statistics in this category include root-mean-square error (RMSE), correlation coefficient (CC), and mean absolute error (MAE), which are calculated by the following equations:

$$\mathrm{RMSE} = \frac{1}{n}\sqrt{\sum_{i=1}^{n}(\mathrm{Sim}_i - \mathrm{Obs}_i)^2},$$

$$\mathrm{CC} = \frac{\frac{1}{n}\sum_{i=1}^{n}(\mathrm{Sim}_i - \overline{\mathrm{Sim}_i})(\mathrm{Obs}_i - \overline{\mathrm{Obs}_i})}{\sigma_{\mathrm{Sim}}\sigma_{\mathrm{Obs}}},$$

$$\mathrm{MAE} = \frac{1}{n}\sum_{i=1}^{n}|\mathrm{Sim}_i - \mathrm{Obs}_i|,$$

where "Sim" is simulation (PERSIANN-CCS, PERSIANN-SDAE, PERSIANN-CNN) and "Obs" is ground reference observation (Stage IV).

4. Results and discussion

a. *Performance evaluation at hourly scale*

An extreme storm that occurred on 3 August 2013 over the study area is examined to compare the performance of PERSIANN-CNN against PERSIANN-CCS and PERSIANN-SDAE. At 1100 UTC 3 August 2013, two separate cloud patches can be detected using the IR (Fig. 4a) and WV channels (Fig. 4b), which show intense rainfalls mostly near the central areas of the larger patch (Fig. 4c). As shown in Fig. 4e, PERSIANN-CNN provides a more realistic representation of the extent and the pattern of the rainfall patches (Fig. 4c) as compared to PERSIANN-CCS (Fig. 4f) and PERSIANN-SDAE (Fig. 4d). Both PERSIANN-SDAE and PERSIANN-CCS falsely detect precipitation occurrence over the majority of the larger cloud patch where the cloud temperature is relatively lower. Also, PERSIANN-CNN is more accurate than the other two models in identifying the location of the rainfall patches. This can be observed by looking at the location of the smaller rainfall patch, where the PERSIANN-SDAE estimates seems to have a northward shift. PERSIANN-CNN gives more accurate intensity estimates compared with PERSIANN-SDAE and PERSIANN-CCS (Figs. 4d,f), which underestimate and overestimate, respectively. Overall, Fig. 4 demonstrates that PERSIANN-CNN is capable of providing more accurate estimates of the shape, location, and intensity of precipitation in comparison to PERSIANN-CCS and PERSIANN-SDAE. Similar maps for another case study (0900 UTC 16 August 2013) also demonstrate the superior performance of PERSIANN-CNN in detecting the precipitation spatial pattern and the magnitude (Fig. 5).These observations can be justified based on the models' structures. PERSIANN-SDAE employs a pixel-based approach that does not leverage the neighborhood information efficiently. In specific, SDAE links all of the pixels of IR and WV to all of the hidden neurons in the autoencoder algorithm. This architecture known as a fully connected network makes it hard to efficiently and effectively learn the structure of the rainy patches and thus estimate the correct shapes

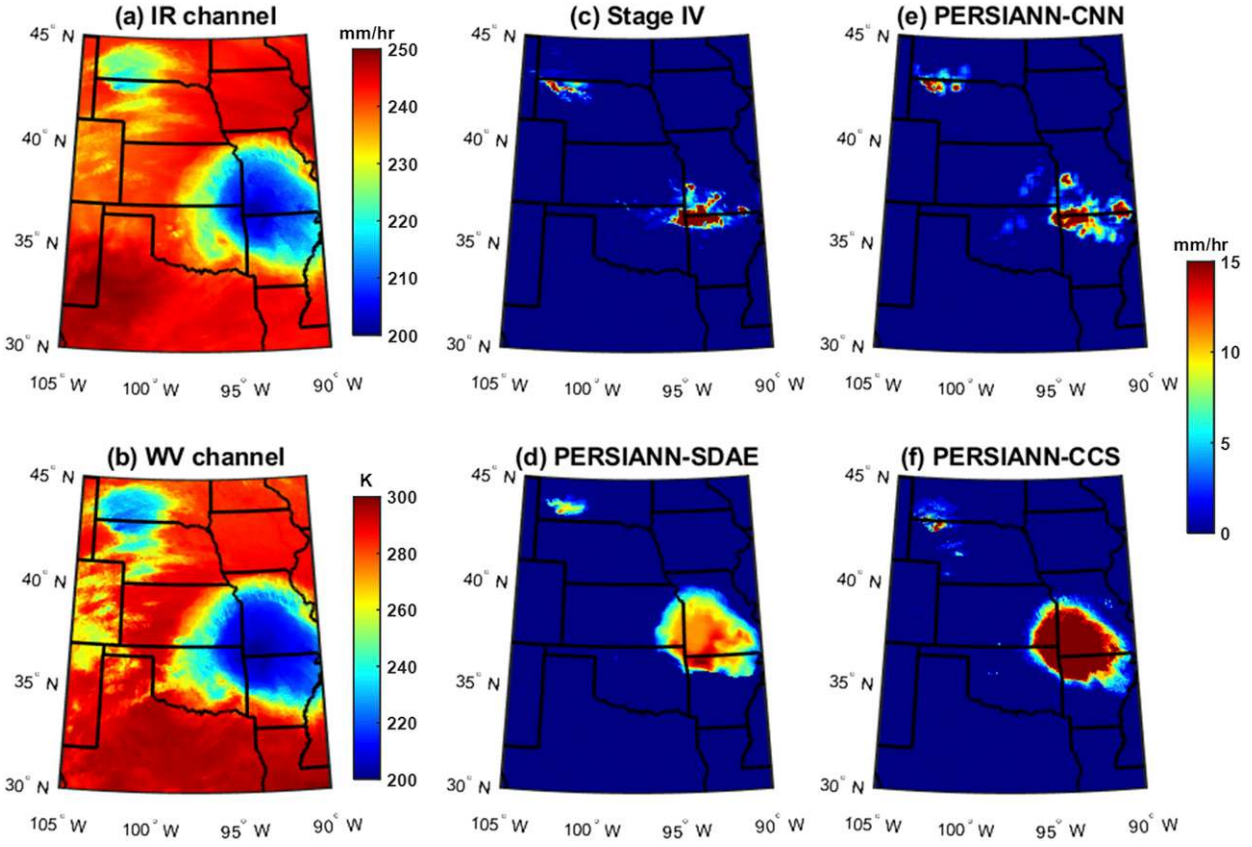

FIG. 4. Case study I: Maps of cloud-top temperature (K) from (a) IR imagery and (b) WV imagery, and precipitation rate (mm h^{-1}) from (c) Stage IV radar observation, (d) PERSIANN-SDAE, (e) PERSIANN-CNN, and (f) PERSIANN-CCS for 1100 UTC 3 Aug 2013.

and rainfall rates. Due to the higher complexity level of fully connected networks for learning spatially correlated data (i.e., images), they tend to restrict the learning to one-on-one pixels in most cases, meaning that they train the parameters of each pixel separately. In addition, in most cases due to the fuzzy and patchy nature of rainfall spatial structure, the SDAE model cannot effectively link neighborhood information. Therefore, SDAE learns an indirect relationship between the cloud temperature and the rain rate, resulting in colder clouds showing more intense precipitation and in larger patches of rainfall compared to ground-truth radar observations. On the other hand, PERSIANN-CCS is a patch-based approach which classifies each rainfall event based on its cold cloud patches and the patch features; however, in the last step of the algorithm which is the rainfall mapping step (i.e., nonlinear regression), a fully connected layer is assigned to find the relationship of infrared brightness temperature and rainfall rates. The same deficiencies of the above-explained fully connected for SDAE apply to the rainfall mapping step of PERSIANN-CCS also resulting in estimating larger patches of rainfall compared to ground-truth radar observations.

Table 1 summarizes the performance of each model in terms of categorical (POD, FAR, and CSI) and continuous (MAE, RMSE, and CC) metrics throughout the verification period of August 2013. All verification metrics were computed for each pixel and at hourly time scale over the study area for the entire verification period. In addition, Fig. 6 presents the spatial distribution of the mentioned metrics of the PERSIANN-CNN and the two baseline models for the verification period. In general, PERSIANN-CNN shows substantial improvement compared to PERSIANN-CCS and PERSIANN-SDAE according to the performance metrics. Compared to the baseline models, PERSIANN-CNN shows a significant improvement in POD and CSI, especially in the central and western regions of the study area. For FAR, the performance of the PERSIANN-CNN and PERSIANN-SDAE is almost the same and obviously better than PERSIANN-CCS, which is also obvious from the FAR values presented in Table 1. Furthermore, PERSIANN-CNN calculates more accurate rainfall intensity estimates as evident by its lower MAE, RMSE, and higher CORR values during the verification period (Table 1 and Fig. 6). As shown in the

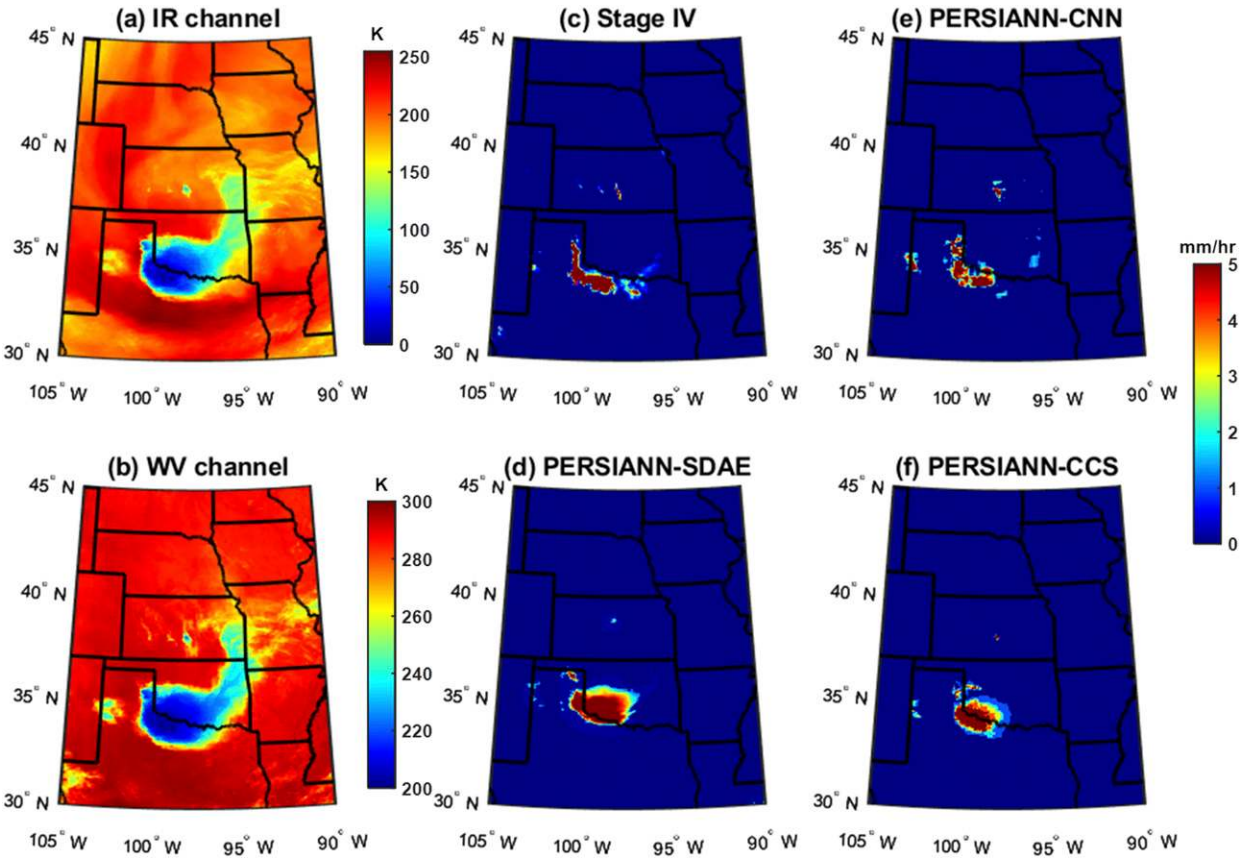

FIG. 5. Case study II: Maps of cloud-top temperature (K) from (a) IR imagery and (b) WV imagery, and precipitation rate (mm h^{-1}) from (c) Stage IV, (d) PERSIANN-SDAE, (e) PERSIANN-CNN, and (f) PERSIANN-CCS snapshots for 0900 UTC 16 Aug 2013.

figures, PERSIANN-CNN performance metrics are more homogeneous compared to PERSIANN-CCS and PERSIANN-SDAE across space over the whole study area. This spatial homogeneity is more noticeable in the spatial pattern of FAR where PERSIANN-CNN performs almost the same for the entire study area while PERSIANN-SDAE performs well in some areas and poor for other parts. This shows the capability of the PERSIANN-CNN to generalize features across spatial domains; conversely, PERSIANN-CCS and PERSIANN-SDAE show diverse performances metrics across the case-study area, showing their localized features. The localized performance of PERSIANN-SDAE is partially due to selecting a small and fixed portion of study area for the training samples of the model (Tao et al. 2018).

b. *Performance evaluation at daily scale*

The proposed model, PERSIANN-CNN, was also evaluated and compared with the baseline models at a daily time scale. To do so, hourly estimates were accumulated to daily values for the extreme event that occurred from 3 to 10 August 2013. According to the National Weather Service, heavy rainfalls were observed in various locations across Missouri, southeast Kansas, and Arkansas from 3 to 10 August 2013 (https://www.weather.gov/sgf/events_2013aug3). Rainfall rates of around 5 mm h^{-1} are reported across these areas for several days, receiving between 20 and 25 mm accumulated rain in a short window of time in some locations. This extreme amount of precipitation resulted in flash flooding causing three deaths with many water rescues and hundreds of flooded roadways in those areas. Specifically on 3 August, an

TABLE 1. Summary of hourly precipitation estimation performance for discussed models over the test periods. Bold text indicates the numbers that are better in terms of performance (higher values for POD, CSI, and CC and lower values for FAR, MAE, and RMSE).

	POD	FAR	CSI	MAE (mm)	RMSE (mm h^{-1})	CC
PERSIANN-CCS	0.39	0.66	0.24	0.19	1.40	0.22
PERSIANN-SDAE	0.45	**0.52**	0.30	0.14	1.02	0.28
PERSIANN-CNN	**0.67**	0.56	**0.37**	**0.12**	**0.88**	**0.41**

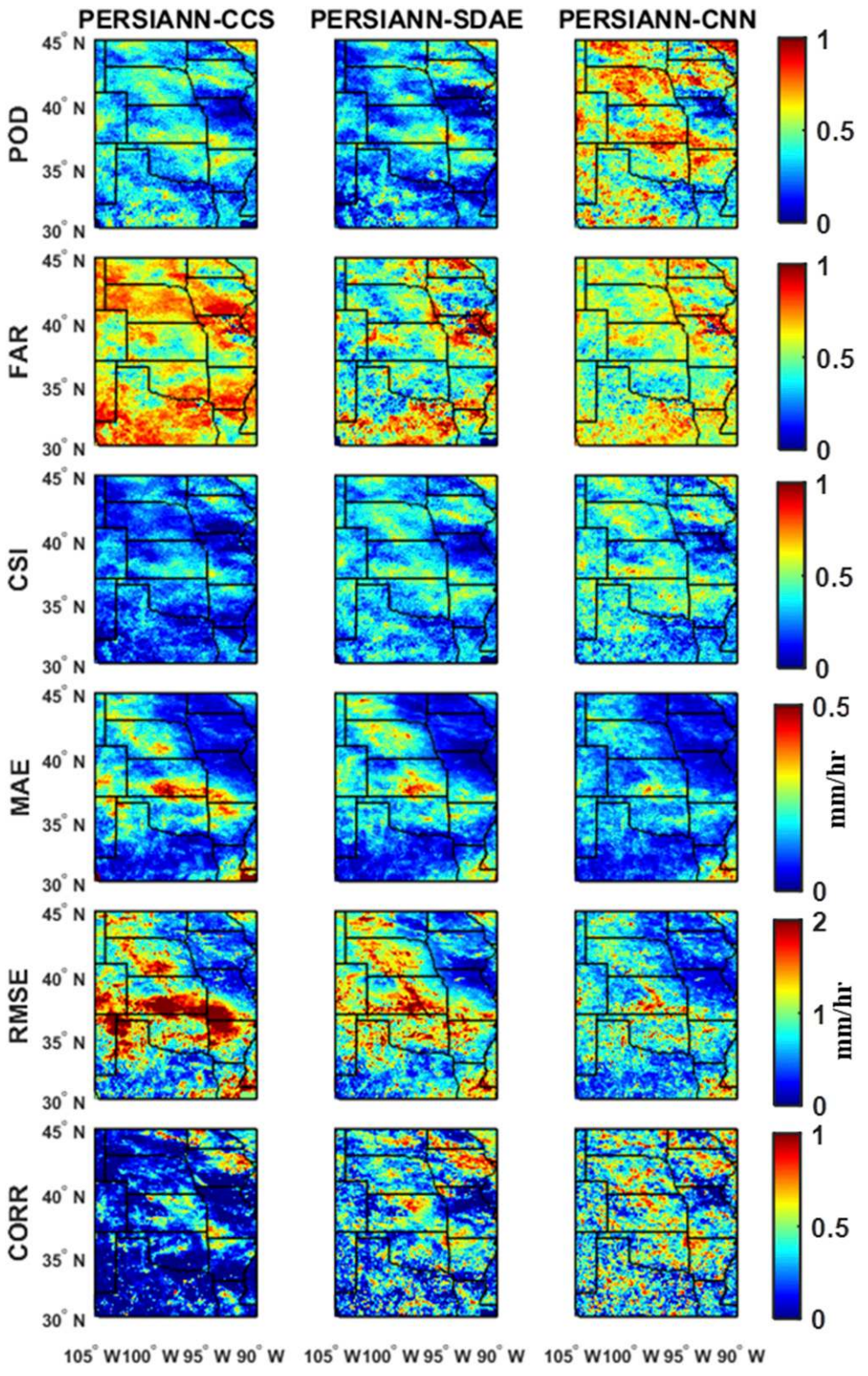

FIG. 6. Categorical (POD, FAR, CSI) and continuous (MAE, RMSE, CORR) metrics of PERSIANN-CCS, PERSIANN-SDAE, and PERSIANN-CNN over the entire verification period.

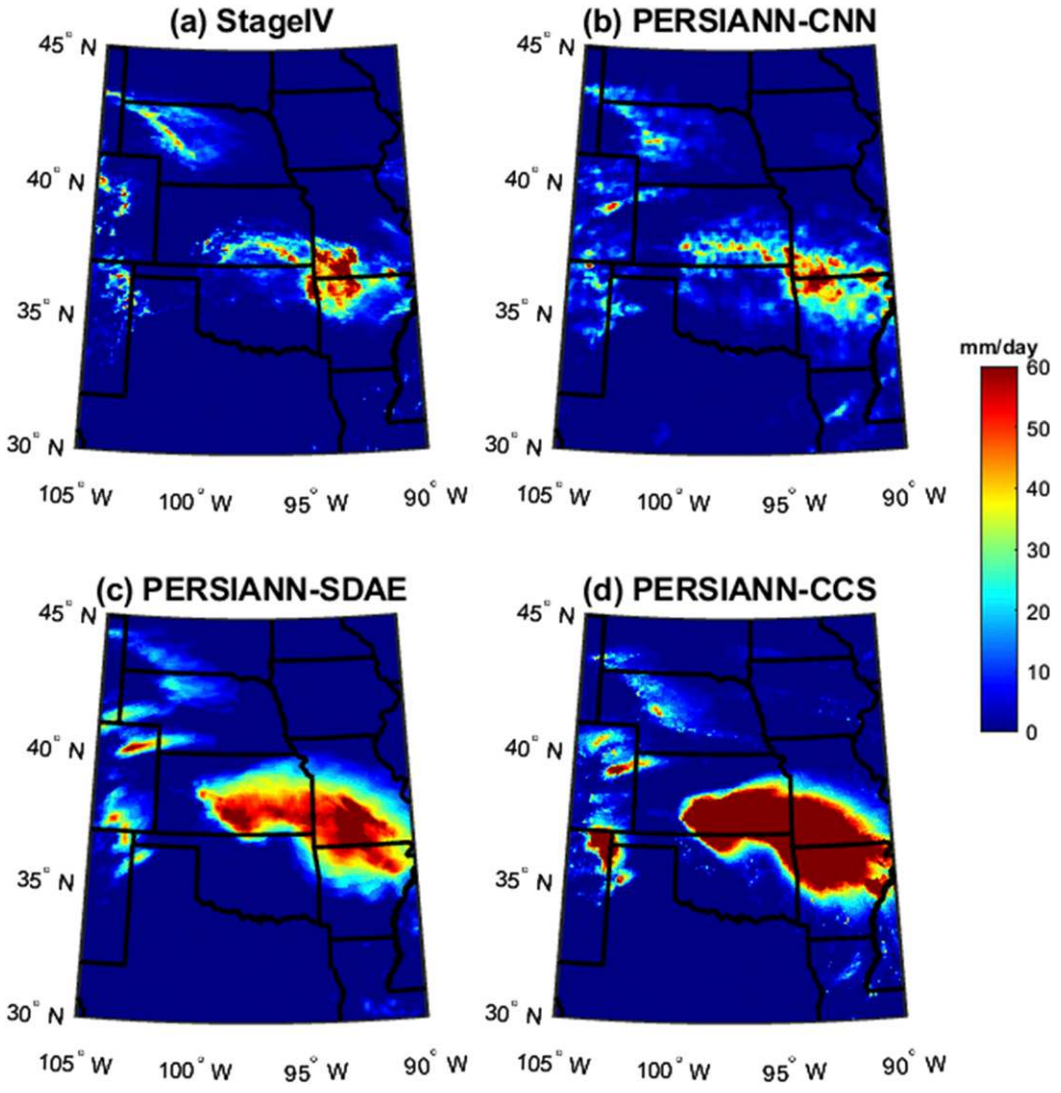

FIG. 7. Comparison of daily rainfall from radar, PERSIANN-CNN, PERSIANN-SDAE, and PERSIANN CCS estimates at 0.08° for 3 Aug 2013.

extreme heavy rainfall occurred in Missouri, Kansas, and Arkansas with an intensity of approximately 5 mm h^{-1}, lasting almost 12 h from 0400 to 1500 UTC (https://www.weather.gov/ict/event_08042013). Some areas received between 40 and 60 mm of precipitation in a short period of time. This considerable amount of rainfall triggered dangerous flash floods, with lots of property damages.

Figures 7 and 8 present the daily values for the extreme precipitation event that occurred on 3 and 10 August 2013, respectively. In both cases PERSIANN-CNN provides a more accurate detection of the rainfall pattern compared to the baseline models. Furthermore, the spatial variation of the PERSIANN-CNN estimation for this day is more similar to that of the radar observations than the PERSIANN-CCS and PERSIANN-SDAE estimations. For the extreme event on 3 August, both PERSIANN-CCS and PERSIANN-SDAE overestimate the rain rate and assign heavy rainfall to larger areas, while PERSIANN-CNN provides a more realistic representation of heavy rainfall areas (Fig. 7). For the 10 August event, the peak of heavy extreme rainfall can be observed mostly at the northern part of Arkansas State (Fig. 8). PERSIANN-CCS captures both the spatial pattern and intensity of the rainfall fairly well. On the other hand, PERSIANN-CCS and PERSIANN-SDAE underestimate the rain rate. In addition, a northward shifting can be seen in PERSIANN-SDAE's estimates.

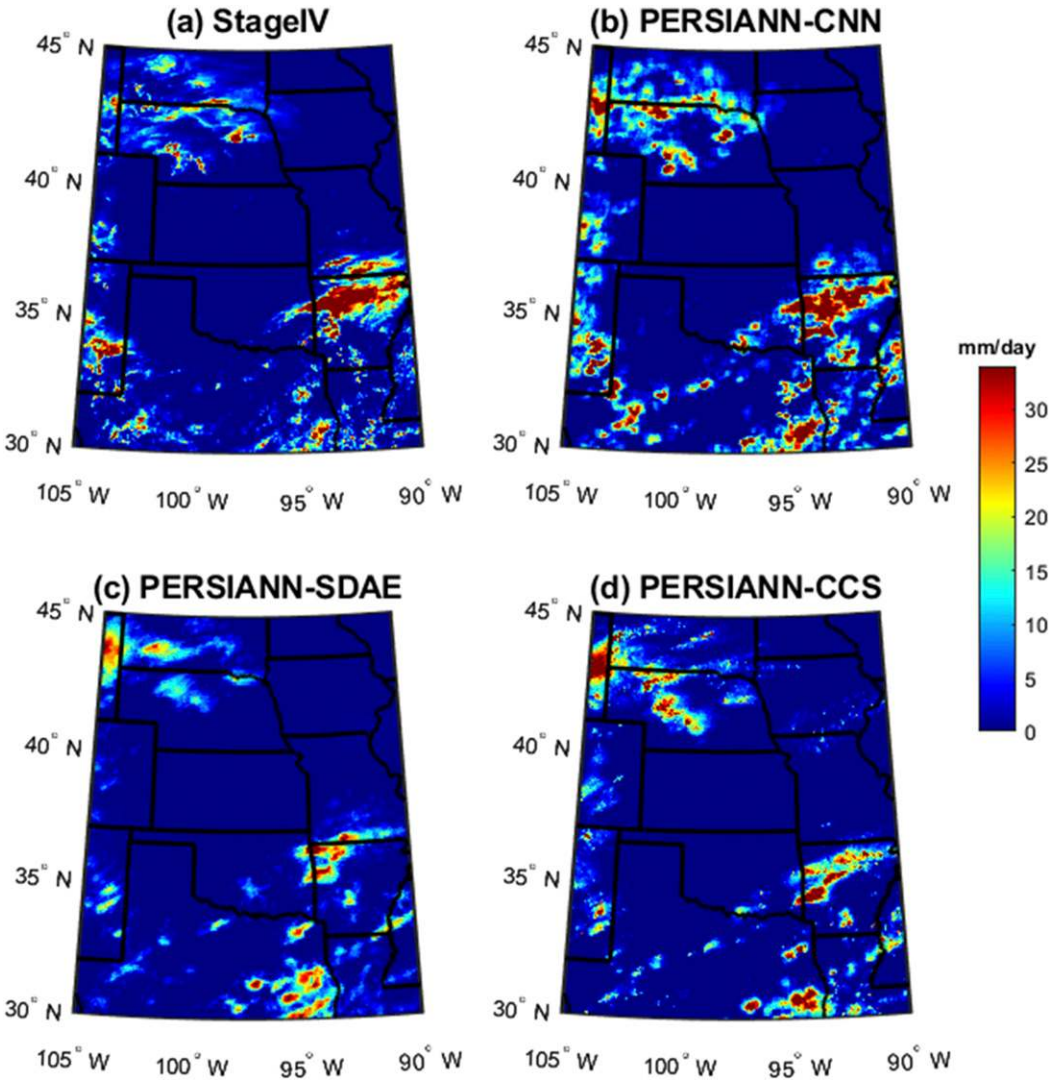

FIG. 8. Comparison of daily rainfall from radar, PERSIANN-CNN, PERSIANN-SDAE, and PERSIANN CCS estimates at 0.08° for 10 Aug 2013.

These two daily case studies emphasize the superior of the CNN-based model compared to the baseline models in terms of accurately estimating the rainfall distribution. Similar to the hourly performance, PERSIANN-CNN estimates the spatial pattern and volumetric of the rainfall more accurately than the baseline models due to its efficient structure. In addition, although PERSIANN-SDAE uses KL divergence, which was utilized for preserving the rainfall distribution, along with MSE as the loss functions, PERSIANN-CNN can perform better only by applying the MSE loss function in the training process. This indicates that CNN-based models can effectively learn features for preserving the spatial and volumetric distribution of precipitation during the training process without needing to add some other terms to the loss function.

Figure 9 demonstrates how the proposed model and the baseline models perform in detecting and estimating the rainfall intensity throughout the different evolution stages of the intense storm that occurred over latitude 34°–38°N and longitude 90°–100°W on 3 August 2013. Time series plots for the hourly rainfall estimates by the radar observations, PERSIANN-CNN, PERSIANN-CCS, and PERSIANN-SDAE are shown in Fig. 9a. PERSIANN-CCS and PERSIANN-SDAE overestimate the rainfall for the entire event. However, PERSIANN-CNN's estimates correspond well with the radar observations although there is a slight overestimation and underestimation before and after 1100 UTC, respectively. The time series plot of the CC (Fig. 9b) reveals that PERSIANN-CNN's estimates have higher correlation with Stage IV radar observations during the event

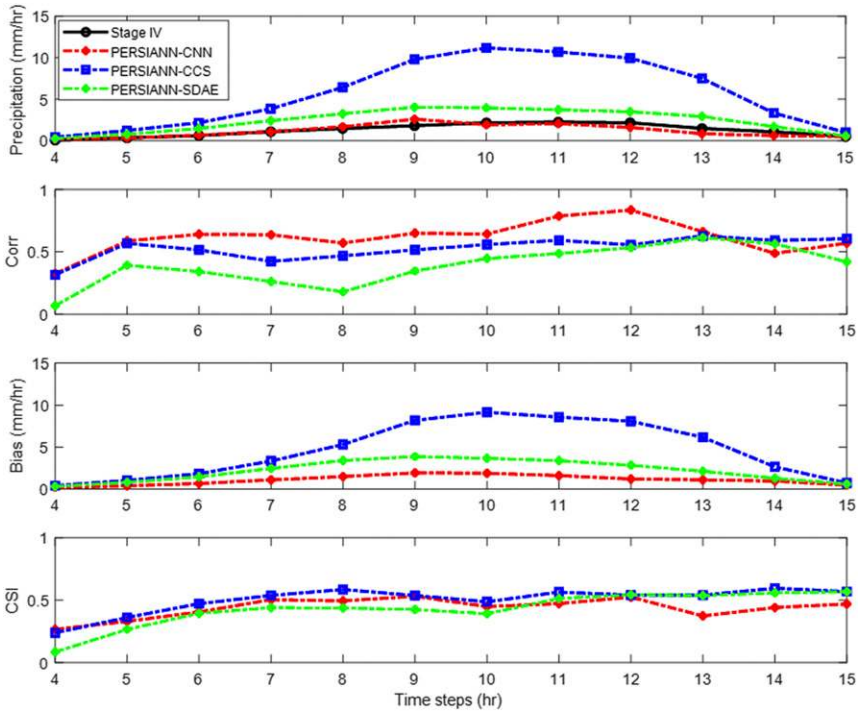

FIG. 9. Time series plots of (a) hourly rainfall estimates, (b) correlation coefficient, (c) bias ($mm\,h^{-1}$), and (d) CSI derived from Stage IV radar observation, PERSIANN-CCS, PERSIANN-SDAE, and PERSIANN-CNN throughout the evolution of the storm event from 0400 to 1500 UTC 3 Aug 2013.

compared to PERSIANN-CCS and PERSIANN-SDAE. PERSIANN-CCS and PERSIANN-SDAE demonstrate positive bias ratios with maximums of approximately 10 and $4\,mm\,h^{-1}$, respectively (Fig. 9c), However, the bias ratio for PERSIANN-CNN (approximately $1\,mm\,h^{-1}$) is noticeably less than that of the baseline models. For detection skill (Fig. 9d), all of the models perform more or less the same, each outperforming the other two models at some stages of the storm's evolution.

To explore the daily performance of PERSIANN-CNN against PERSIANN-CCS and PERSIANN-SDAE at various spatial resolutions, scatterplots of their daily precipitation estimation versus the radar observations for 3 August 2013 are presented (Fig. 10). These figures demonstrate the pixel by pixel association between the satellite-based estimates and the radar observations for various spatial resolutions and at daily time scale. As shown, during the described extreme event on 3 August 2013, both PERSIANN-CNN and PERSIANN-CCS show a high correlation (0.75) with the radar observations at 0.08° spatial resolution. However, RMSE and MAE for PERSIANN-CCS are relatively higher than for PERSIANN-CNN and PERSIANN-SDAE. Furthermore, it can be seen that PERSIANN-CCS tends to overestimate intense precipitation in all spatial resolutions, while PERSIANN-SDAE and PERSIANN-CNN tend to underestimate rain rates at both 0.08° and 0.16° resolution, but underestimation of heavy precipitation is improved as the resolution decreases to 0.25° and 0.5°.

5. Conclusions

In this study, the application of convolutional neural networks (CNNs) in detecting and estimating precipitation from bispectral satellite imagery (IR and WV channels) was explored. A case study over the central United States was conducted to assess the effectiveness of the presented model at 0.08° spatial for both hourly and daily temporal resolution. The proposed model was evaluated against Stage IV radar observations and two existing satellite datasets, PERSIANN-CCS and PERSIANN-SDAE.

Model evaluation procedures at hourly and daily scales showed that PERSIANN-CNN outperforms PERSIANN-CCS and PERSIANN-SDAE in capturing the extent and shape of the rainfall patches by providing a more realistic representation of the precipitation pattern. Model evaluation during the verification period showed that the proposed model performs better than the baseline models in rainfall detection.

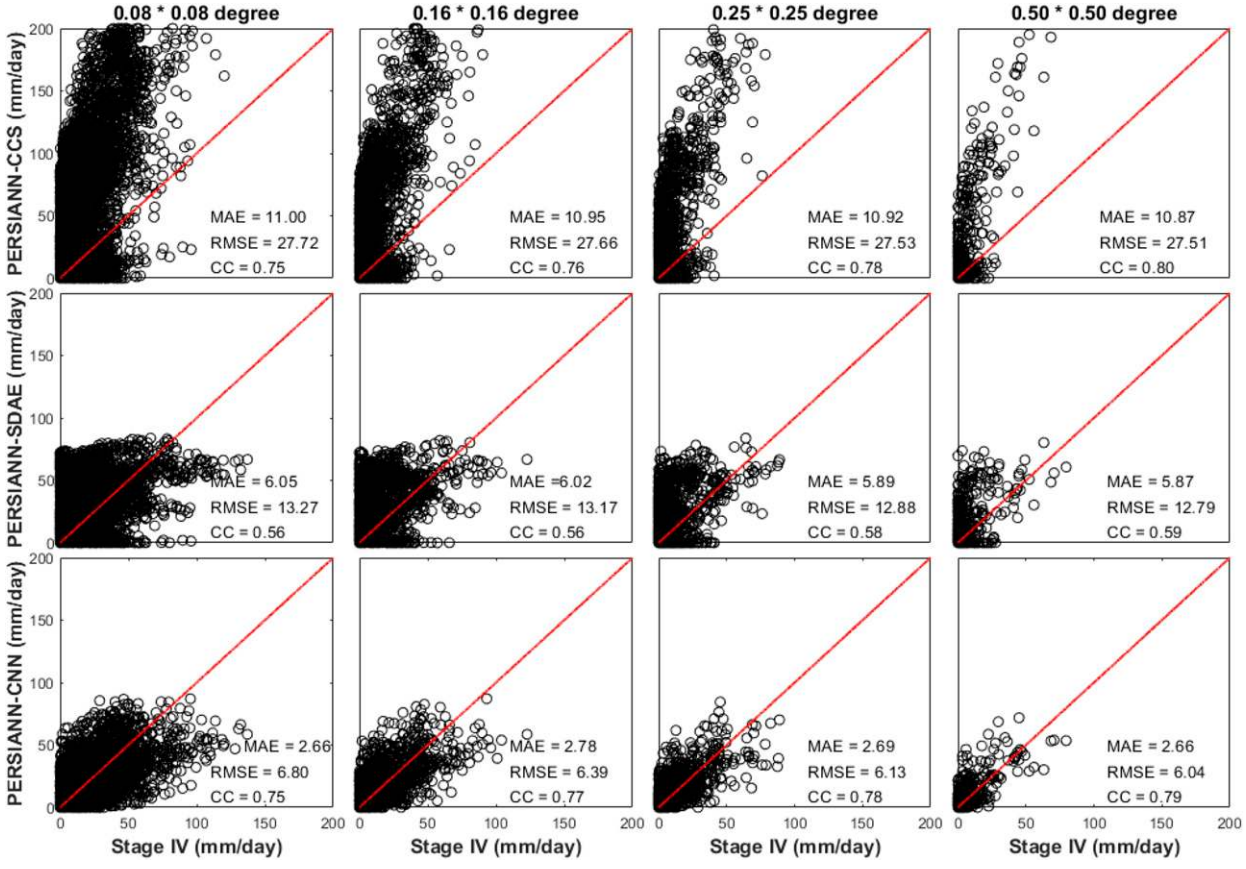

FIG. 10. Scatterplots of radar measurements vs PERSIANN-CCS, PERSIANN-SDAE, and PERSIANN-CNN: daily rainfall estimation at four spatial scales for the study area on 3 Aug 2013.

In terms of POD and CSI, PERSIANN-CNN outperformed PERSIANN-CCS (PERSIANN-SDAE) by 72% (49%) and 54% (23%), respectively. In terms of FAR, PERSIANN-CNN performed better than PERSIANN-SDAE by 12%; however, it performed poorer than PERSIANN-CCS by 10%. Despite the lower performance of PERSIANN-CNN for FAR compared to PERSIANN-SDAE, PERSIANN-CNN has a more homogeneous and consistent performance for the various evaluation metrics, especially FAR. Additionally, the proposed model had the best overall performance in estimation accuracy over the verification period. For RMSE and MAE, PERSIANN-CNN was more accurate than PERSIANN-CCS (PERSIANN-SDAE) by 37% (14%) and 8% (74%) respectively.

To assess the performance of the models in estimating extreme precipitation, a storm event that affected the central United States in August 2013 was selected. Results indicate that PERSIANN-CNN can capture the spatial shape and peak values of rainfalls more precisely than the baseline models according to the RMSE and MAE indices. Furthermore, rain rate time series demonstrated better overall performance by PERSIANN-CNN. Specifically, the proposed model gave the closest approximations to Stage IV radar for the hourly rainfall, as well as the lowest bias values across the hourly time steps. Finally, a pixel-by-pixel performance evaluation of the PERSIANN-CNN and baseline models with respect to the radar observations was implemented at various spatial resolutions (0.08°, 0.16°, 0.25°, and 0.5°). Results of this analysis demonstrated that PERSIANN-CNN and PERSIANN-CCS show higher correlation (0.75) with the radar observations at 0.08° spatial resolution compared to PERSIANN-SDAE. However, RMSE and MAE of PERSIANN-CCS are relatively higher than PERSIANN-CNN and PERSIANN-SDAE. In addition PERSIANN-CCS overestimates the rain rate for all spatial resolutions, while PERSIANN-CNN and PERSIANN-SDAE tended to underestimate very intense precipitation at a high spatial resolution; however, their underestimations of extreme precipitation were improved as the spatial resolution decreased.

Expanding on the research presented here, researchers at the Center for Hydrometeorology and Remote Sensing (CHRS) will implement the framework to a larger spatial extent with longer verification periods to investigate the stability of the model. The presented model's skill in capturing meaningful IR features can leverage PMW information to better describe the precipitation phenomenon. We are currently extending the proposed model to provide near-real-time global precipitation estimation using PMW information as observation for training the model. In addition, NOAA's latest GOES-R Series satellites will provide data at higher temporal and spatial resolutions for use in the model framework.

Acknowledgments. The financial support of this research is from the U.S. Department of Energy (DOE Prime Award DE-IA0000018), the California Energy Commission (CEC Award 300-15-005), MASEEH fellowship, the NSF Project (Award CCF-1331915), NOAA/NESDIS/NCDC (Prime Award NA09NES4400006 and NCSU CICS and Subaward 2009-1380-01), the U.S. Army Research Office (Award W911NF-11-1-0422) and the National Key R&D Program of China (Grant 2016YFE0102400).

REFERENCES

Akbari Asanjan, A., T. Yang, K. Hsu, S. Sorooshian, J. Lin, and Q. Peng, 2018: Short-term precipitation forecast based on the PERSIANN system and LSTM recurrent neural networks. *J. Geophys. Res. Atmos.*, **123**, 12 543–12 563, https://doi.org/10.1029/2018JD028375.

Aoki, P.M., 2017: CNNs for precipitation estimation from geostationary satellite imagery. CS 231N Project Rep., 9 pp., http://cs231n.stanford.edu/reports/2017/pdfs/557.pdf.

Arkin, P. A., and B. N. Meisner, 1987: The relationship between large-scale convective rainfall and cold cloud over the Western Hemisphere during 1982–84. *Mon. Wea. Rev.*, **115**, 51–74, https://doi.org/10.1175/1520-0493(1987)115<0051:TRBLSC>2.0.CO;2.

Assem, H., S. Ghariba, G. Makrai, P. Johnston, L. Gill, and F. Pilla, 2017: Urban water flow and water level prediction based on deep learning. *Machine Learning and Knowledge Discovery in Databases*: *ECML PKDD 2017*, Y. Altun et al., Eds., Lecture Notes in Computer Science, Vol. 10536. Springer, 317–329, https://doi.org/10.1007/978-3-319-71273-4_26.

Ba, M. B., and A. Gruber, 2001: GOES Multispectral Rainfall Algorithm (GMSRA). *J. Appl. Meteor.*, **40**, 1500–1514, https://doi.org/10.1175/1520-0450(2001)040<1500:GMRAG>2.0.CO;2.

Basaeed, E., H. Bhaskar, P. Hill, M. Al-Mualla, and D. Bull, 2016: A supervised hierarchical segmentation of remote-sensing images using a committee of multi-scale convolutional neural networks. *Int. J. Remote Sens.*, **37**, 1671–1691, https://doi.org/10.1080/01431161.2016.1159745.

Beck, H. E., and Coauthors, 2017: Global-scale evaluation of 22 precipitation datasets using gauge observations and hydrological modeling. *Hydrol. Earth Syst. Sci.*, **21**, 6201–6217, https://doi.org/10.5194/hess-21-6201-2017.

Behrangi, A., K.-l. Hsu, B. Imam, S. Sorooshian, G. J. Huffman, and R. J. Kuligowski, 2009: PERSIANN-MSA: A precipitation estimation method from satellite-based multispectral analysis. *J. Hydrometeor.*, **10**, 1414–1429, https://doi.org/10.1175/2009JHM1139.1.

Bellerby, T., M. Todd, D. Kniveton, and C. Kidd, 2000: Rainfall estimation from a combination of TRMM precipitation radar and GOES multispectral satellite imagery through the use of an artificial neural network. *J. Appl. Meteor.*, **39**, 2115–2128, https://doi.org/10.1175/1520-0450(2001)040<2115:REFACO>2.0.CO;2.

Bengio, Y., P. Lamblin, D. Popovici, and H. Larochelle, 2007: Greedy layer-wise training of deep networks. *Proceedings of the 19th International Conference on Neural Information Processing Systems*, MIT Press, 153–160.

Castelluccio, M., G. Poggi, C. Sansone, and L. Verdoliva, 2015: Land use classification in remote sensing images by convolutional neural networks. arXiv, https://arxiv.org/abs/1508.00092.

Chen, Y., Z. Lin, X. Zhao, G. Wang, and Y. Gu, 2014: Deep learning-based classification of hyperspectral data. *IEEE J. Sel. Top. Appl. Earth Obs. Remote Sens.*, **7**, 2094–2107, https://doi.org/10.1109/JSTARS.2014.2329330.

——, H. Jiang, C. Li, X. Jia, and P. Ghamisi, 2016: Deep feature extraction and classification of hyperspectral images based on convolutional neural networks. *IEEE Trans. Geosci. Remote Sens.*, **54**, 6232–6251, https://doi.org/10.1109/TGRS.2016.2584107.

Erhan, D., Y. Bengio, A. Courville, P.-A. Manzagol, P. Vincent, and S. Bengio, 2010: Why does unsupervised pre-training help deep learning? *J. Mach. Learn. Res.*, **11**, 625–660.

Gehne, M., T. M. Hamill, G. N. Kiladis, and K. E. Trenberth, 2016: Comparison of global precipitation estimates across a range of temporal and spatial scales. *J. Climate*, **29**, 7773–7795, https://doi.org/10.1175/JCLI-D-15-0618.1.

Germann, U., G. Galli, M. Boscacci, and M. Bolliger, 2006: Radar precipitation measurement in a mountainous region. *Quart. J. Roy. Meteor. Soc.*, **132**, 1669–1692, https://doi.org/10.1256/qj.05.190.

Grecu, M., W. S. Olson, and E. N. Anagnostou, 2004: Retrieval of precipitation profiles from multiresolution, multifrequency active and passive microwave observations. *J. Appl. Meteor.*, **43**, 562–575, https://doi.org/10.1175/1520-0450(2004)043<0562:ROPPFM>2.0.CO;2.

Guo, H., S. Chen, A. Bao, J. Hu, A. Gebregiorgis, X. Xue, and X. Zhang, 2015: Inter-comparison of high-resolution satellite precipitation products over Central Asia. *Remote Sens.*, **7**, 7181–7211, https://doi.org/10.3390/rs70607181.

Habib, E., A. T. Haile, Y. Tian, and R. J. Joyce, 2012: Evaluation of the high-resolution CMORPH satellite rainfall product using dense rain gauge observations and radar-based estimates. *J. Hydrometeor.*, **13**, 1784–1798, https://doi.org/10.1175/JHM-D-12-017.1.

Hinton, G. E., S. Osindero, and Y.-W. Teh, 2006: A fast learning algorithm for deep belief nets. *Neural Comput.*, **18**, 1527–1554, https://doi.org/10.1162/neco.2006.18.7.1527.

Hong, Y., K.-L. Hsu, S. Sorooshian, and X. Gao, 2004: Precipitation Estimation from Remotely Sensed Imagery Using an Artificial Neural Network Cloud Classification System. *J. Appl. Meteor.*, **43**, 1834–1853, https://doi.org/10.1175/JAM2173.1.

Houze, R. A., Jr., 2012: Orographic effects on precipitating clouds. *Rev. Geophys.*, **50**, RG1001, https://doi.org/10.1029/2011RG000365.

Hsu, K., X. Gao, S. Sorooshian, and H. V. Gupta, 1997: Precipitation Estimation from Remotely Sensed Information Using Artificial Neural Networks. *J. Appl. Meteor.*, **36**, 1176–1190, https://doi.org/10.1175/1520-0450(1997)036<1176:PEFRSI>2.0.CO;2.

Huffman, G. J., and Coauthors, 1997: The Global Precipitation Climatology Project (GPCP) combined precipitation dataset. *Bull. Amer. Meteor. Soc.*, **78**, 5–20, https://doi.org/10.1175/1520-0477(1997)078<0005:TGPCPG>2.0.CO;2.

——, R. F. Adler, M. M. Morrissey, D. T. Bolvin, S. Curtis, R. Joyce, B. McGavock, and J. Susskind, 2001: Global precipitation at one-degree daily resolution from multisatellite observations. *J. Hydrometeor.*, **2**, 36–50, https://doi.org/10.1175/1525-7541(2001)002<0036:GPAODD>2.0.CO;2.

Joyce, R. J., J. E. Janowiak, P. A. Arkin, and P. Xie, 2004: CMORPH: A method that produces global precipitation estimates from passive microwave and infrared data at high spatial and temporal resolution. *J. Hydrometeor.*, **5**, 487–503, https://doi.org/10.1175/1525-7541(2004)005<0487:CAMTPG>2.0.CO;2.

Kidd, C., and V. Levizzani, 2011: Status of satellite precipitation retrievals. *Hydrol. Earth Syst. Sci.*, **15**, 1109–1116, https://doi.org/10.5194/hess-15-1109-2011.

Krizhevsky, A., I. Sutskever, and G. E. Hinton, 2012: ImageNet classification with deep convolutional neural networks. *Proceedings of the 25th International Conference on Neural Information Processing Systems*, Curran Associates, 1097–1105.

Kurino, T., 1997: A satellite infrared technique for estimating ''deep/shallow'' precipitation. *Adv. Space Res.*, **19**, 511–514, https://doi.org/10.1016/S0273-1177(97)00063-X.

Längkvist, M., A. Kiselev, M. Alirezaie, and A. Loutfi, 2016: Classification and segmentation of satellite orthoimagery using convolutional neural networks. *Remote Sens.*, **8**, 329, https://doi.org/10.3390/rs8040329.

Lary, D. J., A. H. Alavi, A. H. Gandomi, and A. L. Walker, 2016: Machine learning in geosciences and remote sensing. *Geosci. Front.*, **7**, 3–10, https://doi.org/10.1016/j.gsf.2015.07.003.

Lin, Y., and K. E. Mitchell, 2005: The NCEP Stage II/IV hourly precipitation analyses: Development and applications. *19th Conf. on Hydrology*, San Diego, CA, Amer. Meteor. Soc., 1.2, https://ams.confex.com/ams/Annual2005/techprogram/paper_83847.htm.

Liu, Y., E. Racah, J. Correa, A. Khosrowshahi, D. Lavers, K. Kunkel, M. Wehner, and W. Collins, 2016: Application of deep convolutional neural networks for detecting extreme weather in climate datasets. arXiv, https://arxiv.org/abs/1605.01156.

Long, Y., Y. Gong, Z. Xiao, and Q. Liu, 2017: Accurate object localization in remote sensing images based on convolutional neural networks. *IEEE Trans. Geosci. Remote Sens.*, **55**, 2486–2498, https://doi.org/10.1109/TGRS.2016.2645610.

Luus, F. P., B. P. Salmon, F. Van den Bergh, and B. T. J. Maharaj, 2015: Multiview deep learning for land-use classification. *IEEE Geosci. Remote Sens. Lett.*, **12**, 2448–2452, https://doi.org/10.1109/LGRS.2015.2483680.

Maggioni, V., P. C. Meyers, and M. D. Robinson, 2016: A review of merged high-resolution satellite precipitation product accuracy during the Tropical Rainfall Measuring Mission (TRMM) era. *J. Hydrometeor.*, **17**, 1101–1117, https://doi.org/10.1175/JHM-D-15-0190.1.

Makantasis, K., K. Karantzalos, A. Doulamis, and N. Doulamis, 2015: Deep supervised learning for hyperspectral data classification through convolutional neural networks. *2015 IEEE Int. Geoscience and Remote Sensing Symp.*, Milan, Italy, IEEE, 4959–4962, https://doi.org/10.1109/IGARSS.2015.7326945.

Marzano, F. S., M. Palmacci, D. Cimini, G. Giuliani, and F. J. Turk, 2004: Multivariate statistical integration of satellite infrared and microwave radiometric measurements for rainfall retrieval at the geostationary scale. *IEEE Trans. Geosci. Remote Sens.*, **42**, 1018–1032, https://doi.org/10.1109/TGRS.2003.820312.

Miao, C., H. Ashouri, K.-L. Hsu, S. Sorooshian, and Q. Duan, 2015: Evaluation of the PERSIANN-CDR daily rainfall estimates in capturing the behavior of extreme precipitation events over China. *J. Hydrometeor.*, **16**, 1387–1396, https://doi.org/10.1175/JHM-D-14-0174.1.

Miao, Q., B. Pan, H. Wang, K. Hsu, and S. Sorooshian, 2019: Improving monsoon precipitation prediction using combined convolutional and long short term memory neural network. *Water*, **11**, 977, https://doi.org/10.3390/w11050977.

Michaelides, S., V. Levizzani, E. Anagnostou, P. Bauer, T. Kasparis, and J. Lane, 2009: Precipitation: Measurement, remote sensing, climatology and modeling. *Atmos. Res.*, **94**, 512–533, https://doi.org/10.1016/j.atmosres.2009.08.017.

Pan, B., K. Hsu, A. AghaKouchak, and S. Sorooshian, 2018: Improving precipitation estimation using convolutional neural network. *Water Resour. Res.*, **55**, 2301–2321, https://doi.org/10.1029/2018WR024090.

Pradhan, R., R. S. Aygun, M. Maskey, R. Ramachandran, and D. J. Cecil, 2018: Tropical cyclone intensity estimation using a deep convolutional neural network. *IEEE Trans. Image Process.*, **27**, 692–702, https://doi.org/10.1109/TIP.2017.2766358.

Rezaee, M., M. Mahdianpari, Y. Zhang, and B. Salehi, 2018: Deep convolutional neural network for complex wetland classification using optical remote sensing imagery. *IEEE J. Sel. Top. Appl. Earth Obs. Remote Sens.*, **11**, 3030–3039, https://doi.org/10.1109/JSTARS.2018.2846178.

Roebeling, R., and I. Holleman, 2009: SEVIRI rainfall retrieval and validation using weather radar observations. *J. Geophys. Res.*, **114**, D21202, https://doi.org/10.1029/2009JD012102.

Salberg, A.-B., 2015: Detection of seals in remote sensing images using features extracted from deep convolutional neural networks. 2015 *IEEE Int. Geoscience and Remote Sensing Symp.*, Milan, Italy, IEEE, 1893–1896, https://doi.org/10.1109/IGARSS.2015.7326163.

Ševo, I., and A. Avramović, 2016: Convolutional neural network based automatic object detection on aerial images. *IEEE Geosci. Remote Sens. Lett.*, **13**, 740–744, https://doi.org/10.1109/LGRS.2016.2542358.

Shen, C., 2018: A transdisciplinary review of deep learning research and its relevance for water resources scientists. *Water Resour. Res.*, **54**, 8558–8593, https://doi.org/10.1029/2018WR022643.

Smalley, M., T. L'Ecuyer, M. Lebsock, and J. Haynes, 2014: A comparison of precipitation occurrence from the NCEP Stage IV QPE product and the CloudSat Cloud Profiling Radar. *J. Hydrometeor.*, **15**, 444–458, https://doi.org/10.1175/JHM-D-13-048.1.

Sorooshian, S., K.-L. Hsu, X. Gao, H. V. Gupta, B. Imam, and D. Braithwaite, 2000: Evaluation of PERSIANN system satellite-based estimates of tropical rainfall. *Bull. Amer. Meteor. Soc.*, **81**, 2035–2046, https://doi.org/10.1175/1520-0477(2000)081<2035:EOPSSE>2.3.CO;2.

——, X. Gao, K. Hsu, R. Maddox, Y. Hong, H. V. Gupta, and B. Imam, 2002: Diurnal variability of tropical rainfall retrieved from combined GOES and TRMM satellite information.

J. Climate, **15**, 983–1001, https://doi.org/10.1175/1520-0442(2002)015<0983:DVOTRR>2.0.CO;2.

Stohl, A., and P. James, 2004: A Lagrangian analysis of the atmospheric branch of the global water cycle. Part I: Method description, validation, and demonstration for the August 2002 flooding in central Europe. *J. Hydrometeor.*, **5**, 656–678, https://doi.org/10.1175/1525-7541(2004)005<0656:ALAOTA>2.0.CO;2.

Sun, Q., C. Miao, Q. Duan, H. Ashouri, S. Sorooshian, and K. L. Hsu, 2018: A review of global precipitation data sets: Data sources, estimation, and intercomparisons. *Rev. Geophys.*, **56**, 79–107, https://doi.org/10.1002/2017RG000574.

Tao, Y., X. Gao, K. Hsu, S. Sorooshian, and A. Ihler, 2016: A deep neural network modeling framework to reduce bias in satellite precipitation products. *J. Hydrometeor.*, **17**, 931–945, https://doi.org/10.1175/JHM-D-15-0075.1.

——, ——, A. Ihler, S. Sorooshian, and K. Hsu, 2017: Precipitation identification with bispectral satellite information using deep learning approaches. *J. Hydrometeor.*, **18**, 1271–1283, https://doi.org/10.1175/JHM-D-16-0176.1.

——, K. Hsu, A. Ihler, X. Gao, and S. Sorooshian, 2018: A two-stage deep neural network framework for precipitation estimation from Bispectral satellite information. *J. Hydrometeor.*, **19**, 393–408, https://doi.org/10.1175/JHM-D-17-0077.1.

Trenberth, K. E., A. Dai, R. M. Rasmussen, and D. B. Parsons, 2003: The changing character of precipitation. *Bull. Amer. Meteor. Soc.*, **84**, 1205–1218, https://doi.org/10.1175/BAMS-84-9-1205.

Van Doorn, J., 2014: Analysis of deep convolutional neural network architectures. *21st Twente Student Conf. on IT,* Enschede, Netherlands, University of Twente, 7 pp.

Vincent, P., H. Larochelle, Y. Bengio, and P.-A. Manzagol, 2008: Extracting and composing robust features with denoising autoencoders. *Proc. 25th Int. Conf. on Machine Learning*, Helsinki, Finland, ACM, 1096–1103, https://doi.org/10.1145/1390156.1390294.

Walker, I., M. Deisenroth, and A. Faisal, 2015: Deep convolutional neural networks for brain computer interface using motor imagery. MSc. thesis, Imperial College London, 68 pp., http://www.doc.ic.ac.uk/~mpd37/theses/DeepEEG_IanWalker2015.pdf.

Weng, F., L. Zhao, R. R. Ferraro, G. Poe, X. Li, and N. C. Grody, 2003: Advanced microwave sounding unit cloud and precipitation algorithms. *Radio Sci.*, **38**, 8068, https://doi.org/10.1029/2002RS002679.

Yang, J., M. N. Nguyen, P. P. San, X. L. Li, and S. Krishnaswamy, 2015: Deep convolutional neural networks on multichannel time series for human activity recognition. Proc. 24th Int. Joint Conf. on Artificial Intelligence, Buenos Aires, Argentina, IJCAI, 3995–4001, https://www.ijcai.org/Proceedings/15/Papers/561.pdf.

Yilmaz, K. K., T. S. Hogue, K.-l. Hsu, S. Sorooshian, H. V. Gupta, and T. Wagener, 2005: Intercomparison of rain gauge, radar, and satellite-based precipitation estimates with emphasis on hydrologic forecasting. *J. Hydrometeor.*, **6**, 497–517, https://doi.org/10.1175/JHM431.1.

Zhu, X. X., D. Tuia, L. Mou, G.-S. Xia, L. Zhang, F. Xu, and F. Fraundorfer, 2017: Deep learning in remote sensing: A comprehensive review and list of resources. *IEEE Geosci. Remote Sens. Mag.*, **5**, 8–36, https://doi.org/10.1109/MGRS.2017.2762307.

Zhuang, W., and W. Ding, 2016: Long-lead prediction of extreme precipitation cluster via a spatiotemporal convolutional neural network. *Proc. Sixth Int. Workshop on Climate Informatics*, Boulder, CO, NCAR, NCAR/TN-529+PROC, 128–131, https://doi.org/10.5065/D6K072N6.